

Rational design and synthesis of $Cr_{1-x}Te/Ag_2Te$ composites for solid-state thermoelectromagnetic cooling near room temperature

Xiaochen Sun(孙笑晨), Chenghao Xie(谢承昊), Sihan Chen(陈思汗), Jingwei Wan(万京伟), Gangjian Tan(谭刚健), and Xinfeng Tang(唐新峰)

Citation: Chin. Phys. B, 2024, 33 (**5**): 057201. DOI: 10.1088/1674-1056/ad2d57
Journal homepage: http://cpb.iphy.ac.cn; http://iopscience.iop.org/cpb

What follows is a list of articles you may be interested in

Ga intercalation in van der Waals layers for advancing p-type Bi_2Te_3-based thermoelectrics

Yiyuan Chen(陈艺源), Qing Shi(石青), Yan Zhong(钟艳), Ruiheng Li(李瑞恒), Liwei Lin(林黎蔚), Ding Ren(任丁), Bo Liu(刘波), and Ran Ang(昂然)
Chin. Phys. B, 2023, 32 (**6**): 067201. DOI: 10.1088/1674-1056/acc2af

Advancing thermoelectrics by suppressing deep-level defects in Pb-doped $AgCrSe_2$ alloys

Yadong Wang(王亚东), Fujie Zhang(张富界), Xuri Rao(饶旭日), Haoran Feng(冯皓然), Liwei Lin(林黎蔚), Ding Ren(任丁), Bo Liu(刘波), and Ran Ang(昂然)
Chin. Phys. B, 2023, 32 (**4**): 047202. DOI: 10.1088/1674-1056/acb765

Large valley Nernst effect in twisted multilayer graphene systems

Guanlin Jian(简冠林), Zhen-Gang Zhu(朱振刚), and Gang Su(苏刚)
Chin. Phys. B, 2023, 32 (**10**): 107202. DOI: 10.1088/1674-1056/acbd2c

Large Seebeck coefficient resulting from chiral interactions in triangular triple quantum dots

Yi-Ming Liu(刘一铭) and Jian-Hua Wei(魏建华)
Chin. Phys. B, 2022, 31 (**9**): 097201. DOI: 10.1088/1674-1056/ac6dae

Micro thermoelectric devices: From principles to innovative applications

Qiulin Liu(刘求林), Guodong Li(李国栋), Hangtian Zhu(朱航天), and Huaizhou Zhao(赵怀周)
Chin. Phys. B, 2022, 31 (**4**): 047204. DOI: 10.1088/1674-1056/ac5609

Rational design and synthesis of $Cr_{1-x}Te/Ag_2Te$ composites for solid-state thermoelectromagnetic cooling near room temperature

Xiaochen Sun(孙笑晨)[1], Chenghao Xie(谢承昊)[1], Sihan Chen(陈思汗)[1], Jingwei Wan(万京伟)[1,2], Gangjian Tan(谭刚健)[1,†], and Xinfeng Tang(唐新峰)[1,‡]

[1] *State Key Laboratory of Advanced Technology for Materials Synthesis and Processing, Wuhan University of Technology, Wuhan* 430070, *China*
[2] *International School of Materials Science & Engineering, Wuhan University of Technology, Wuhan* 430070, *China*

(Received 28 January 2024; revised manuscript received 20 February 2024; accepted manuscript online 27 February 2024)

Materials with both large magnetocaloric response and high thermoelectric performance are of vital importance for all-solid-state thermoelectromagnetic cooling. These two properties, however, hardly coexist in single phase materials except previously reported hexagonal $Cr_{1-x}Te$ half metal where a relatively high magnetic entropy change ($-\Delta S_M$) of ~ 2.4 J·kg^{-1}·K^{-1} @ 5 T and a moderate thermoelectric figure of merit (ZT) of $\sim 1.2\times10^{-2}$ @ 300 K are simultaneously recorded. Herein we aim to increase the thermoelectric performance of $Cr_{1-x}Te$ by compositing with semiconducting Ag_2Te. It is discovered that the *in-situ* synthesis of $Cr_{1-x}Te/Ag_2Te$ composites by reacting their constitute elements above melting temperatures is unsuccessful because of strong phase competition. Specifically, at elevated temperatures ($T >$ 800 K), $Cr_{1-x}Te$ has a much lower deformation energy than Ag_2Te and tends to become more Cr-deficient by capturing Te from Ag_2Te. Therefore, Ag is insufficiently reacted and as a metal it deteriorates ZT. We then rationalize the synthesis of $Cr_{1-x}Te/Ag_2Te$ composites by *ex-situ* mix of the pre-prepared $Cr_{1-x}Te$ and Ag_2Te binary compounds followed by densification at a low sintering temperature of 573 K under a pressure of 3.5 GPa. We show that by compositing with 7 mol% Ag_2Te, the Seebeck coefficient of $Cr_{1-x}Te$ is largely increased while the lattice thermal conductivity is considerably reduced, leading to 72% improvement of ZT. By comparison, $-\Delta S_M$ is only slightly reduced by 10% in the composite. Our work demonstrates the potential of $Cr_{1-x}Te/Ag_2Te$ composites for thermoelectromagnetic cooling.

Keywords: thermoelectromagnetic cooling, thermoelectric, magnetocaloric, composite, chromium telluride

PACS: 72.15.Jf, 73.50.Lw **DOI:** 10.1088/1674-1056/ad2d57

1. Introduction

With the growing greenhouse gas emission and energy crisis that limit the use of traditional liquid refrigerants, there is an increasing demand for solid-state refrigeration materials and technologies.[1–5] Among them, thermoelectric cooling[6–8] enabled by the Peltier effect[9–17] and magnetic cooling led by the magnetocaloric effect[18–28] are the most promising, since they have the advantages of high reliability, no moving parts, compact size, and quiet operation. However, their conversion efficiency is still much lower than conventional mechanical-compression refrigeration, making their commercial use impractical.

In recent years, thermoelectromagnetic refrigeration[29–32] by use of electronic entropy flow and magnetic entropy flow as cooling media has been proposed to revolutionize the solid-state cooling technology with potentially higher conversion efficiency. The key point of thermoelectromagnetic refrigeration is to develop new functional materials with both large magnetic entropy change ($-\Delta S_M$) and high thermoelectric figure of merit (ZT).[33] However, these two properties are usually contradictory to each other in a single phase compound, since excellent magneto-thermal materials are mainly ferromagnetic (FM) metals,[34] while most efficient thermoelectric materials are generally doped narrow-bandgap semiconductors.[35,36] There are only a very few exceptions, one of which is $Cr_{1-x}Te$ half metal.[37,38] By varying x, there are a series of binary chromium tellurides with different crystal structures and physical properties. Specifically, when $x \leq 0.09$, $Cr_{1-x}Te$ crystallizes in a hexagonal NiAs-type structure.[39,40] It shows a ferro-to-paramagnetic phase transition at a Curie temperature (T_C) of 334 K.[41] As x is increased to 1/6, the resultant Cr_5Te_6 compound is stabilized in a monoclinic structure with a slightly lower T_C of 326 K. Further increasing x leads to the formation of monoclinic Cr_3Te_4 ($x = 1/4$) and hexagonal Cr_2Te_3 ($x = 1/3$), both of which have T_C lower than 250 K.[42] Most recently, it has been experimentally demonstrated that $Cr_{0.91}Te$ possesses a relatively high $-\Delta S_M$ of ~ 2.4 J·kg^{-1}·K^{-1} under an external magnetic field of 5 T and a moderate ZT of $\sim 1.2\times10^{-2}$ around 300 K.[37] Nonetheless, there is still plenty of room for its performance optimization since the ZT value is 1–2 orders of magnitude lower than that of commercialized bismuth telluride thermoelectric material. The main drawback that limits the ZT of half metallic $Cr_{1-x}Te$ compounds lies in their poor Seebeck coefficients (room temperature value of ~ 20 μV/K vs. ~ 200 μV/K for optimized $Bi_xSb_{2-x}Te_3$[36,43]).

†Corresponding author. E-mail: gtan@whut.edu.cn
‡Corresponding author. E-mail: tangxf@whut.edu.cn

© 2024 Chinese Physical Society and IOP Publishing Ltd

In this work, we attempt to increase the thermoelectric performance of $Cr_{1-x}Te$ without significantly sacrificing its magnetocaloric properties by compositing with semiconducting material, Ag_2Te, which was chosen for its excellent Seebeck coefficient and low thermal conductivity at room temperature.[44] The composite is rationally synthesized by an *ex-situ* route, namely, the pre-prepared $Cr_{1-x}Te$ and Ag_2Te binary compounds are thoroughly ground and mixed prior to densification by a high pressure method (3.5 GPa) under 573 K. The mild synthesis temperature is vital for the elimination of Ag metal from the final product, because there is a strong phase competition between $Cr_{1-x}Te$ and Ag_2Te when the temperature is above 800 K. It is found that the introduction of 7 mol% Ag_2Te into $Cr_{1-x}Te$ increases the ZT value by 72% as a result of Seebeck coefficient enhancement while $-\Delta S_M$ only shows $\sim 10\%$ reduction in this process. Our work highlights the great potential of exploring composites as high performance thermoelectromagnetic multi-functional materials.

2. Experimental procedures

***In-situ* synthesis** Samples were prepared by high temperature reaction. Specifically, Cr powder (325 mesh, 99.99%), Te powder (325 mesh, 99.999%) and Ag powder (≤ 0.2 μm, 99.99%) were thoroughly mixed according to the molar ratio of $Cr_{0.91}Te$–7%Ag_2Te, cold-pressed into a cylinder, and vacuum sealed into a silica tube. It was then reacted at 1073 K for 12 h followed by quenching in saturated salt water.

***Ex-situ* synthesis** $Cr_{0.91}Te$ (or Cr_5Te_6) and Ag_2Te were respectively prepared at first. The synthesis procedure of $Cr_{0.91}Te$ (or Cr_5Te_6) was the same as the one described above. Ag_2Te was prepared by melting high purity Ag pellets (99.99%) and Te blocks (99.999%) in a 2:1 ratio in vacuum sealed silica tubes at 1323 K for 10 h, followed by slow cooling to room temperature. Then the sample was subjected to annealing at 673 K for 3 d, and further annealing at 373 K for 1 d.

Formation energy calculation The formation energies were calculated based on the density functional theory (DFT). All the calculations were performed using the generalized gradient approximation with PBE functional[45] for the exchange–correlation functional and projector augmented wave potentials as implemented in the Vienna *Ab initio* simulation package (VASP).[46] Quasi harmonic approximation implemented in Phonopy code was used to calculate the temperature dependent free energies.

Sintering The as-prepared $Cr_{0.91}Te$ (or Cr_5Te_6) and Ag_2Te were crushed into fine powders, mixed according to the molar ratio of $Cr_{0.91}Te$–7%Ag_2Te and hand milled in an agate mortar for 1 h. The composites were sintered at 1073 K by a hot pressing method in vacuum under an axial pressure of 80 MPa, or densified by a high pressure (3.5 GPa) method under 573 K.

Measurement and characterization Phase purity was examined by powder x-ray diffraction (XRD, Cu $K\alpha$, X'Pert PRO-PANalytical). The chemical compositions were analyzed by an energy dispersive spectrometer (EDS, JXA-8230/INCA X-Act) on the electron probe micro-analyzer (EPMA, JXA-8230). Procedures for magnetocaloric properties and thermoelectric transport properties measurements can be found in Refs. [47,48]. Hall effect study was performed on a physical property measurement system (PPMS-9, Quantum Design) at 300 K under vacuum. The differential scanning calorimetry (DSC) curves were recorded by a DSC Q20 (TA Instrument, Delaware, PA, USA) instrument.

3. Results and discussion

Figure 1(a) shows the powder XRD patterns of the *in-situ* synthesized sample. Although CrTe and Ag_2Te are present in the final product, there are also some unexpected impurity phases which are most likely Cr_5Te_6 and Ag metal. The presence of Ag_2Te is further verified by DSC analysis. As illustrated in Fig. 1(b), an apparent endothermic peak around 421 K upon heating and an exothermic peak near 410 K during cooling are recorded, which is ascribed to the $\alpha\beta$ phase transition of Ag_2Te.[49]

To elucidate the origin of Cr_5Te_6 and Ag metal in the final product by *in-situ* synthesis, we calculate the temperature dependent formation energies (E_{form}) of $Cr_{0.91}Te$, Cr_5Te_6, and Ag_2Te, and the results are compared in Fig. 2. In the low temperature range ($T_{low} < 500$ K), the three compounds have very close values of E_{form}, indicating that they are able to coexist; in the middle temperature range (500 K $< T_{mid} <$ 800 K), we note that the values of E_{form} for $Cr_{0.91}Te$ and Ag_2Te are still comparable, but the one for Cr_5Te_6 is getting lower. It indicates that $Cr_{0.91}Te$ is prone to phase collapse into Cr_5Te_6 and Cr, while Ag_2Te is stable in this temperature interval; in the high temperature range ($T_{high} > 800$ K), E_{form} decreases in the sequence of Ag_2Te, $Cr_{0.91}Te$ and Cr_5Te_6, indicative of a strong phase competition. Specifically, $Cr_{0.91}Te$ captures Te from Ag_2Te to form more stable Cr_5Te_6, rendering the precipitation of Ag metal, as described in the following chemical formula:

$$Cr_{0.91}Te + 0.092Ag_2Te = 0.182Cr_5Te_6 + 0.184Ag. \quad (1)$$

During the *in-situ* synthesis of $Cr_{0.91}Te$–7%Ag_2Te composite, the elements are reacted at 1073 K (T_{high} region). Then it is not surprising that Cr_5Te_6 and Ag metal are found as impurities in the final product. Based on the above findings, we proceed to *ex-situ* synthesize the composite by mixing the pre-prepared $Cr_{0.91}Te$ and Ag_2Te binary compounds to avoid phase competition at high temperatures.

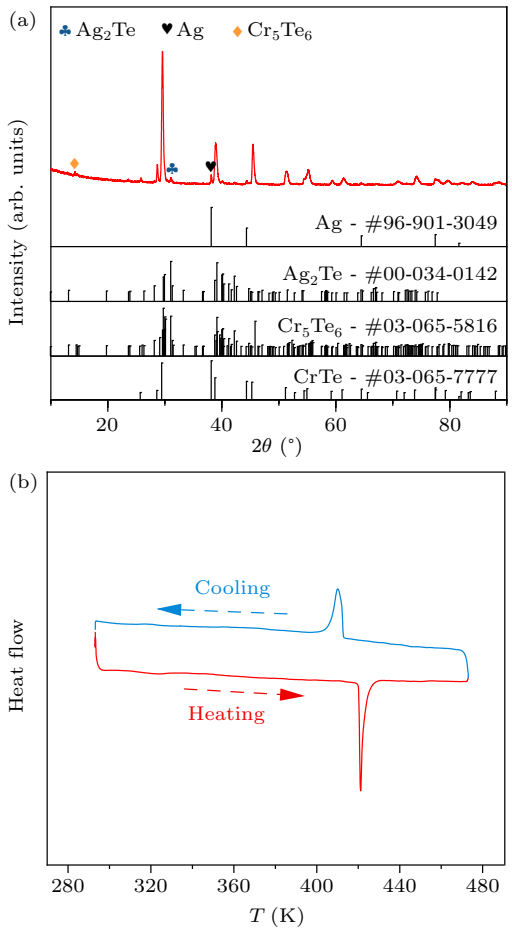


Fig. 1. (a) XRD patterns and (b) DSC curve of *in-situ* synthesized sample.

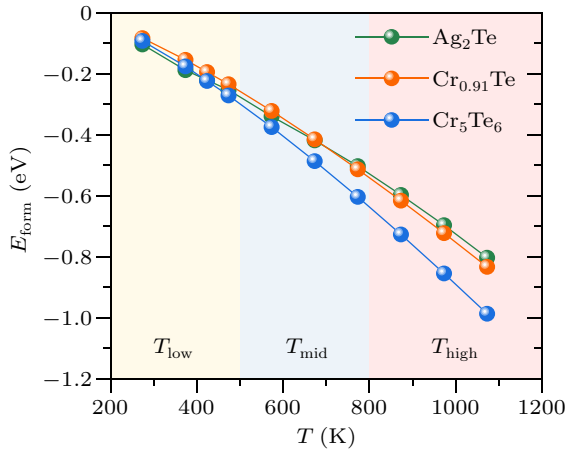


Fig. 2. Temperature dependent formation energy of $Cr_{0.91}Te$, Cr_5Te_6 and Ag_2Te.

Figure 3(a) illustrates the powder XRD patterns of as-synthesized $Cr_{0.91}Te$ and Ag_2Te which are both single phase compounds. After sufficiently grinding at room temperature, their mixture shows no any extra impurity peaks as expected. We proceed to densify the composite by the conventional hot pressing (HP) method for the sake of subsequent thermoelectromagnetic properties measurement. We note a gradual increase of the relative density for the sintered pellets from 85% to 94% and then 97%, when the HP temperature is 873 K, 973 K and 1073 K, respectively. Nonetheless, all samples show the presence of Ag and Cr_5Te_6 impurities in addition to $Cr_{0.91}Te$ and Ag_2Te, as shown in Fig. 3(b). The secondary electron (SE) images, back-scattered electron (BSE) images, and corresponding EDS elemental mappings for the two relatively dense pellets (HP temperatures of 973 K and 1073 K) are displayed in Figs. 3(c) and 3(d), respectively. In both cases, Ag- and Cr-aggregations are clearly observed. For the Ag-aggregations, they are dispersed in two different regions: one has a light grey contrast (highlighted by the dotted blue circles) with lower Te concentration as compared to the matrix, which is assigned to Ag_2Te based on our energy dispersive x-ray analysis; the other one, having almost no phase contrast (highlighted by the dotted golden circles) but featuring the absence of Te, is undoubtedly Ag metal. This is in good agreement with XRD results. The presence of Cr_5Te_6 is not well demonstrated in the EPMA test, probably due to its similar Cr/Te ratio in comparison with that of $Cr_{0.91}Te$. Besides, Cr metals with dark contrast (highlighted by the dotted red circles) are also revealed in our EPMA analysis, though they are not detected by XRD because of their low concentrations. From Fig. 2, we conclude that the high sintering temperature (> 800 K) of HP should be responsible for the observed impurities in the densified pellets. It is of great importance to reduce the sintering temperature of the composite to get rid of undesired impurities after densification.

As we know, both pressure and temperature play crucial roles in the sintering process. Normally, if a higher pressure is applied, a lower sintering temperature could be allowed for full densification. Then we utilize a high pressure (3.5 GPa) method (HPM) in an attempt to compact the composite at sufficiently low temperatures. The pellets are labeled as HPM473, HPM573, HPM673 and HPM773 in terms of their sintering temperatures. As expected, when the sintering temperature is 473 K (namely, within the T_{low} region shown in Fig. 2), the HPM473 pellet has no change of its phase compositions (mixture of $Cr_{0.91}Te$ and Ag_2Te) before and after sintering (Fig. 4(a)). However, its relative density is only $\sim 92\%$, which is unsatisfactory. When the sintering temperature is 573 K or higher (within T_{mid} region), the obtained pellets are fully dense, but they become a mixture of Cr_5Te_6 and Ag_2Te, as noted from the significant right shift and splitting of their diffraction peaks at $2\theta = 37°$ to 43° (Fig. 4(b)). In the meanwhile, Cr metal precipitates out as revealed by the EPMA test for HPM573 (Fig. 4(c)). Therefore, even under 3.5 GPa pressure (the highest one allowed in our apparatus), the lowest sintering temperature for the full densification of $Cr_{0.91}Te$–Ag_2Te composite is still above 500 K. In this T_{mid} region, $Cr_{0.91}Te$ decomposes into Cr_5Te_6 and Cr metal, the latter of which is supposed to be detrimental to thermoelectromagnetic properties.

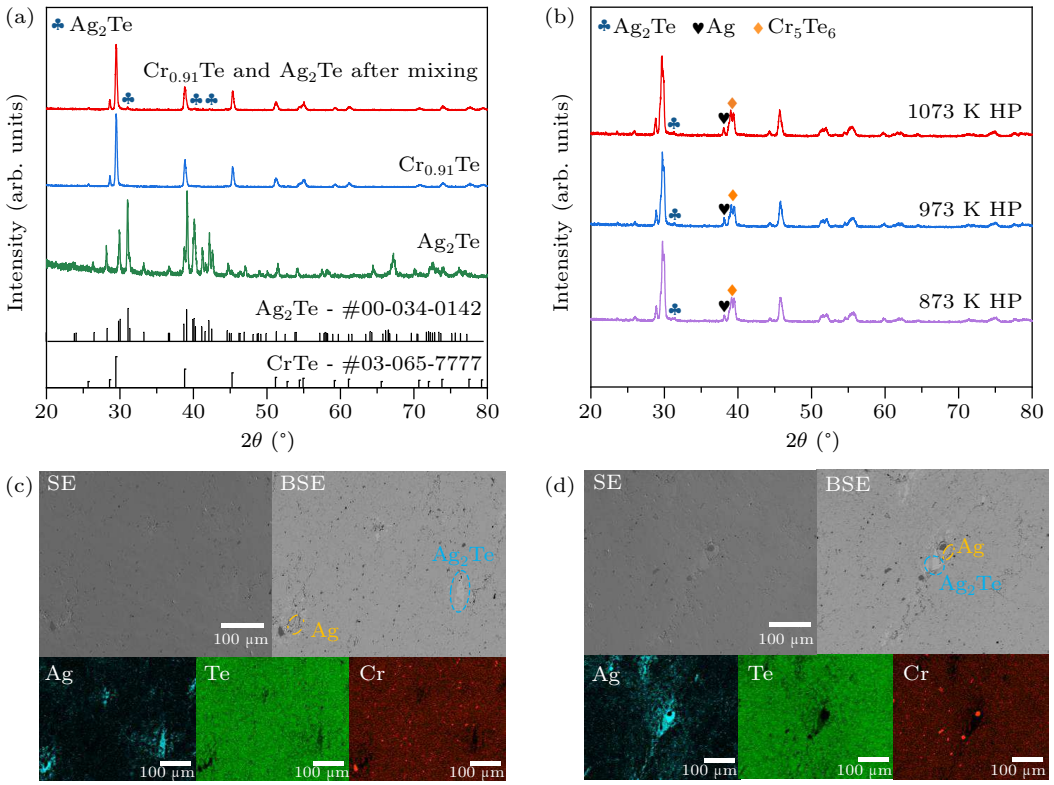


Fig. 3. X-ray powder diffraction patterns of (a) as-synthesized $Cr_{0.91}Te$, Ag_2Te and their mixtures, and (b) $Cr_{0.91}Te$–7%Ag_2Te composite after hot pressing at different temperatures. Secondary electron (SE) images, back-scattered electron (BSE) images, and corresponding EDS elemental mappings for samples hot pressed at (c) 973 K and (d) 1073 K.

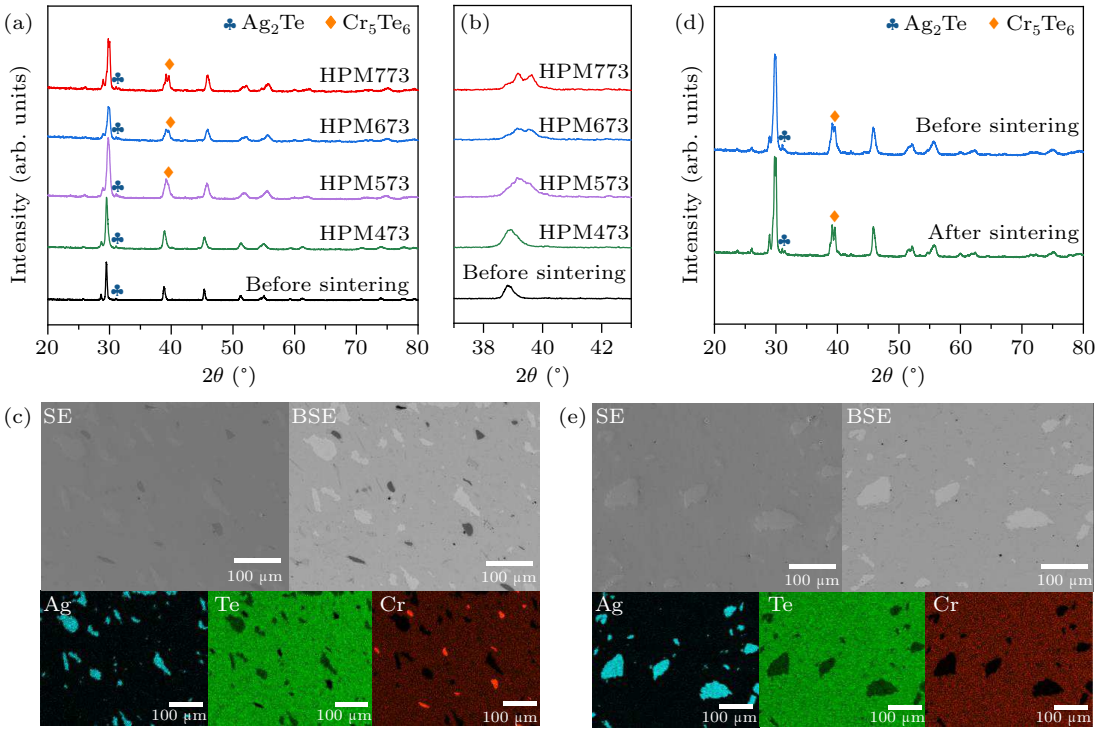


Fig. 4. (a) X-ray powder diffraction patterns of *ex-situ* synthesized $Cr_{0.91}Te$–7%Ag_2Te composite before and after sintering at different temperatures by HPM. (b) Magnification of diffraction peaks at $2\theta = 37°$ to 43° in panel (a). (d) X-ray powder diffraction patterns of Cr_5Te_6–7%Ag_2Te composite before and after sintering at 573 K by HPM. SE images, BSE images, and corresponding EDS elemental mappings for *ex-situ* synthesized (c) $Cr_{0.91}Te$–7%Ag_2Te and (e) Cr_5Te_6–7%Ag_2Te composites after sintering at 573 K by HPM.

Based on the above findings, we decide to optimize the formula of the $Cr_{1-x}Te$–Ag_2Te composite by increasing x from 0.09 to 1/6. In this context, Cr_5Te_6 and Ag_2Te are respectively prepared and then thoroughly mixed at room temperature. They show consistent phase compositions (a mixture of the two components) before and after sintering by HPM at

573 K (Fig. 4(d)). The EPMA analysis shown in Fig. 4(e) reveals the absence of Cr metals in the sintered pellet and the even dispersion of Ag_2Te particles in the Cr_5Te_6 matrix.

The addition of Ag_2Te into Cr_5Te_6 has a profound impact on the thermoelectromagnetic properties. As depicted in Fig. 5, Cr_5Te_6, as a half metal, possesses significantly larger electrical conductivities (σ, Fig. 5(a)) and thermal conductivities (κ, Fig. 5(b)) but lower Seebeck coefficients (S, Fig. 5(c)) than those of semiconducting Ag_2Te over the wide temperature range of interest. Specifically, at room temperature, the values of σ, κ and S for Cr_5Te_6 are 2104 $S\cdot cm^{-1}$, 3.1 $W\cdot m^{-1}\cdot K^{-1}$ and -23 $\mu V\cdot K^{-1}$, respectively, while those for Ag_2Te are 1091 $S\cdot cm^{-1}$, 1.1 $W\cdot m^{-1}\cdot K^{-1}$ and -97 $\mu V\cdot K^{-1}$, respectively. As a composite of the two components, Cr_5Te_6–7%Ag_2Te has intermediate values of all the three physical quantities.

For a random and homogeneous dispersion of the second phase (B, Ag_2Te in this study) in matrix material (A, Cr_5Te_6 herein), the effective electrical conductivity ($\sigma_{\rm eff}$), thermal conductivity ($\kappa_{\rm eff}$) and Seebeck coefficient ($S_{\rm eff}$) of the A–B composite can be estimated by the Bergman–Fel model[50,51]

$$\sigma_{\rm eff} = \sigma_{\rm A} + \frac{\varphi}{D}\left(\frac{\delta_\sigma}{d_{\rm BA}} + \frac{1-\varphi}{3}\frac{\sigma_{\rm A}}{d_{\rm A}}\right), \tag{2}$$

$$\kappa_{\rm eff} = \kappa_{\rm A} + \frac{\varphi}{D}\left(\frac{\delta_\kappa}{d_{\rm BA}} + \frac{1-\varphi}{3}\frac{\kappa_{\rm A}}{d_{\rm A}}\right), \tag{3}$$

$$S_{\rm eff} = \left[S_{\rm A}\sigma_{\rm A} + \frac{\varphi}{D}\left(\frac{\delta_{S\sigma}}{d_{\rm BA}} + \frac{1-\varphi}{3}\frac{S_{\rm A}\sigma_{\rm A}}{d_{\rm A}}\right)\right]\frac{1}{\sigma_{\rm E}}, \tag{4}$$

$$\delta_\sigma \equiv \sigma_{\rm B} - \sigma_{\rm A},\ \ \delta_\kappa \equiv \kappa_{\rm B} - \kappa_{\rm A},\ \ \delta_{S\sigma} \equiv S_{\rm B}\sigma_{\rm B} - S_{\rm A}\sigma_{\rm A}, \tag{5}$$

$$d_{\rm A} \equiv \frac{\sigma_{\rm A}\kappa_{\rm A}}{T} - (S_{\rm A}\sigma_{\rm A})^2,\ \ d_{\rm BA} \equiv \frac{\delta_\sigma\delta_\kappa}{T} - \delta_{S\sigma}^2, \tag{6}$$

$$D \equiv \left(\frac{\delta_\sigma}{d_{\rm BA}} + \frac{1-\varphi}{3}\frac{\sigma_{\rm A}}{d_{\rm A}}\right)\left(\frac{\delta_\kappa}{Td_{\rm BA}} + \frac{1-\varphi}{3}\frac{\kappa_{\rm A}}{Td_{\rm A}}\right) - \left(\frac{\delta_{S\sigma}}{d_{\rm BA}} + \frac{1-\varphi}{3}\frac{S_{\rm A}\sigma_{\rm A}}{d_{\rm A}}\right)^2. \tag{7}$$

In expressions (2)–(7), φ represents the volume fraction of phase B, $\sigma_{\rm A}$ ($\sigma_{\rm B}$), $\kappa_{\rm A}$ ($\kappa_{\rm B}$), and $S_{\rm A}$ ($S_{\rm B}$) denote the electrical conductivity, thermal conductivity and Seebeck coefficient of component A (B), respectively. It is straightforward that the calculated values of σ, κ and S for the Cr_5Te_6–7%Ag_2Te composite agree reasonably with the measured ones. It indicates that Cr_5Te_6 and Ag_2Te are well composited by HPM without serious interdiffusion. Figure 5(d) depicts the calculated thermoelectric figure of merit $ZT = S^2\sigma T/\kappa$. At 300 K, ZT is improved by 72% through compositing, from 0.011 for pristine Cr_5Te_6 to 0.019 after adding 7 mol% Ag_2Te.

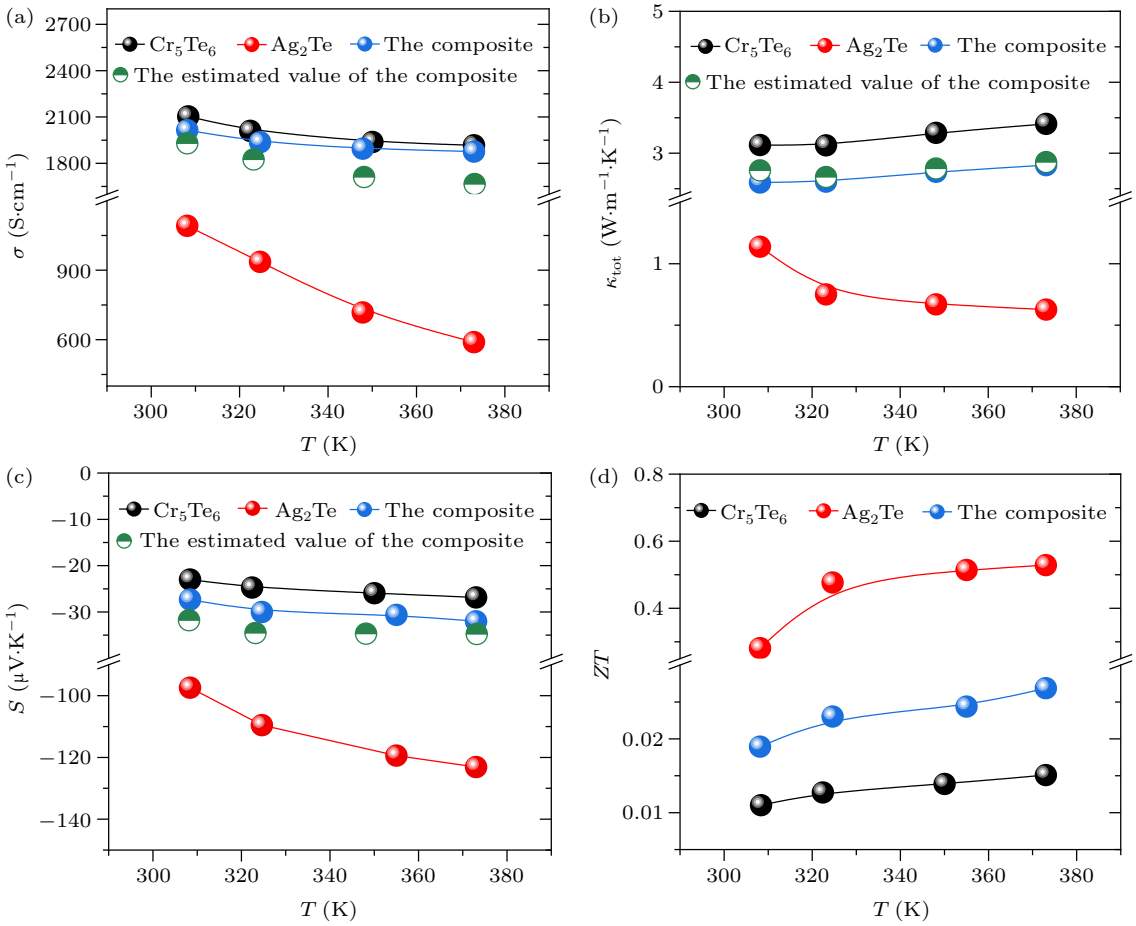


Fig. 5. Temperature dependent (a) electrical conductivity, (b) thermal conductivity, (c) Seebeck coefficient and (d) ZT values for Cr_5Te_6, Ag_2Te, and Cr_5Te_6–7%Ag_2Te composite. The half-filled symbols in panels (a)–(c) are the estimated values of σ, κ and S for the composite under the Bergman–Fel model.

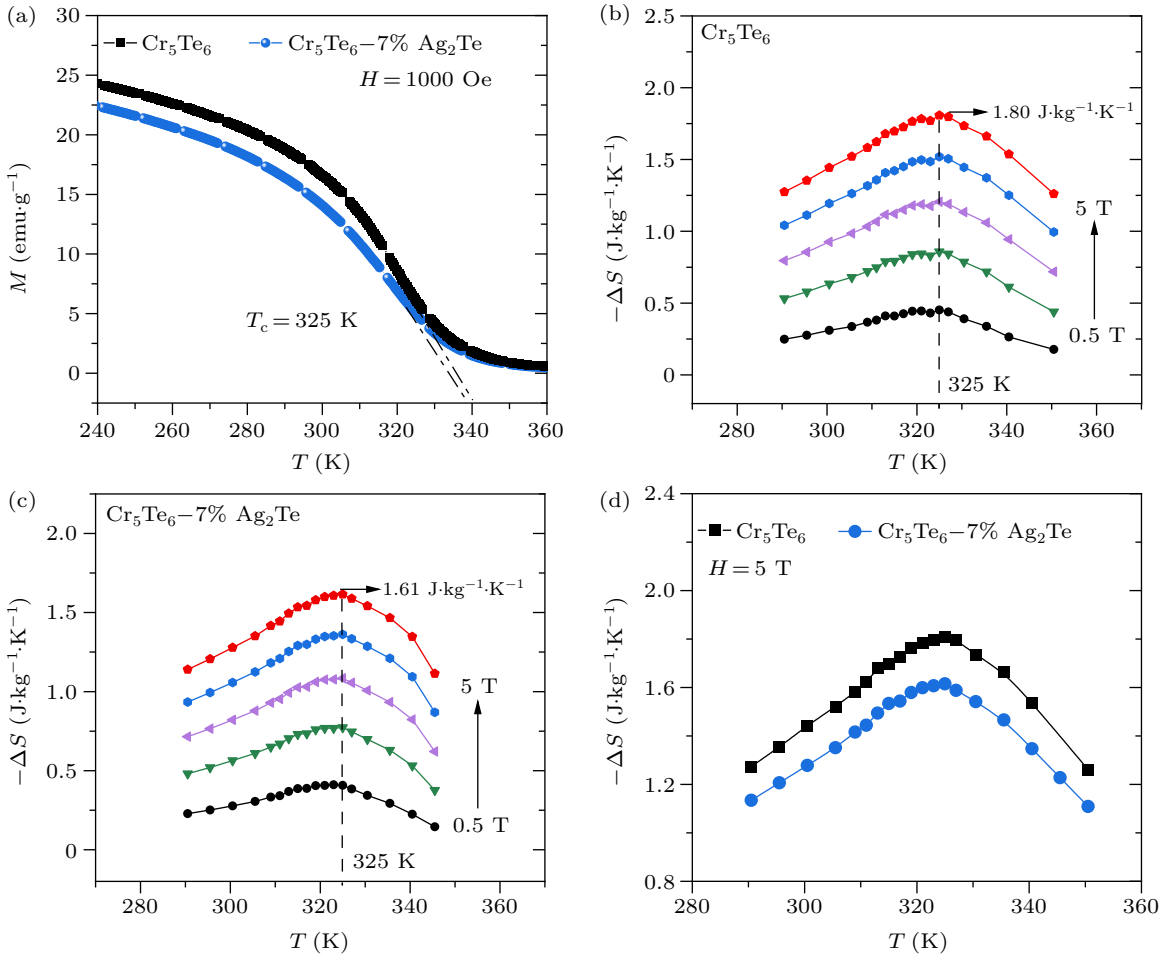


Fig. 6. (a) Temperature dependence of magnetization for Cr_5Te_6 and Cr_5Te_6–7%Ag_2Te. Magnetization isotherms of (b) Cr_5Te_6 and (c) Cr_5Te_6–7%Ag_2Te. (d) Comparisons of temperature dependent magnetic entropy change of Cr_5Te_6 with and without Ag_2Te addition.

The temperature dependent magnetization (M) for pristine Cr_5Te_6 and Cr_5Te_6–7%Ag_2Te composite under a magnetic field (H) of 1000 Oe is illustrated in Fig. 6(a). T_C, defined by the minimum of the dM/dT vs. T curves, is estimated to be $\sim$ 325 K for both samples, which is plausible because Ag_2Te is non-magnetic. Figures 6(b) and 6(c) respectively depict the magnetization isotherms of Cr_5Te_6 and Cr_5Te_6–7%Ag_2Te, from which the temperature dependence of $-\Delta S_M$ under a magnetic field change of 5 T is obtained, and the results are compared in Fig. 6(d). In both cases, $-\Delta S_M$ reaches its peak value around T_C. After adding 7 mol% Ag_2Te, the maximum $-\Delta S_M$ slightly drops by 10%, from 1.80 J·kg^{-1}·K^{-1} for pristine Cr_5Te_6 to 1.61 J·kg^{-1}·K^{-1} for the composite.

4. Conclusion

We show that $Cr_{1-x}Te$ and Ag_2Te have very complex temperature dependence of phase competition, based on which the Cr_5Te_6–Ag_2Te composite was rationally designed and synthesized by an *ex-situ* mix method followed by high pressure sintering. The composite displays intriguing thermoelectromagnetic multi-functional properties. In the vicinity of room temperature, the addition of 7 mol% semiconducting Ag_2Te into half metallic Cr_5Te_6 increases the ZT value remarkably by 72% and decreases $-\Delta S_M$ slightly by 10%. Our work demonstrates the feasibility of exploring ferromagnet-semiconductor composite as advanced thermoelectromagnetic materials for next-generation all-solid-state refrigeration.

Acknowledgments

Project supported by the National Key Research and Development Program of China (Grant No. 2019YFA0704900) and the National Natural Science Foundation of China (Grant No. 52171221).

References

[1] Valant M 2012 *Prog. Mater. Sci.* **57** 980
[2] Takeuchi I and Sandeman K 2015 *Phys. Today* **68** 48
[3] Hong M, Chen Z G and Zou J 2018 *Chin. Phys. B* **27** 048403
[4] Ren Q, Qi J, Yu D, Zhang Z, Song R, Song W, Yuan B, Wang T, Ren W and Zhang Z 2022 *Nat. Commun.* **13** 2293
[5] Li S, Fang X, Lyu T, Cheng J, Ao W, Zhang C, Liu F, Li J and Hu L 2022 *Mater. Today Phys.* **27** 100764
[6] Mao J, Chen G and Ren Z 2021 *Nat. Mater.* **20** 454
[7] Ding J, Zhao W, Jin W, Di C A and Zhu D 2021 *Adv. Funct. Mater.* **31** 2010695
[8] Roychowdhury S, Ghosh T, Arora R, Samanta M, Xie L, Singh N K, Soni A, He J, Waghmare U V and Biswas K 2021 *Science* **371** 722

[9] Tan G, Zhao L D and Kanatzidis M G 2016 *Chem. Rev.* **116** 12123
[10] Enescu D and Virjoghe E O 2014 *Renew. Sust. Energ. Rev.* **38** 903
[11] Zhao D and Tan G 2014 *Appl. Therm. Eng.* **66** 15
[12] Liu Z, Hong T, Xu L, Wang S, Gao X, Chang C, Ding X, Xiao Y and Zhao L D 2023 *Interdiscip. Mater.* **2** 161
[13] Guo H H, Yang T, Tao P and Zhang Z D 2013 *Chin. Phys. B* **23** 017201
[14] Peng P P, Wang C, Li L W, Li S Y and Chen Y Q 2022 *Chin. Phys. B* **31** 047307
[15] Liu H, Zhang X, Li W and Pei Y 2022 *Chin. Phys. B* **31** 047401
[16] Zhao X, Zhao X, Lin L, Ren D, Liu B and Ang R 2022 *Chin. Phys. B* **31** 117202
[17] Yang X, Wang C, Lu R, Shen Y, Zhao H, Li J, Li R, Zhang L, Chen H and Zhang T 2022 *Nano Energy* **101** 107553
[18] Gschneidner J K and Pecharsky V 2008 *Int. J. Refrig.* **31** 945
[19] Tishin A, Spichkin Y, Zverev V and Egolf P 2016 *Int. J. Refrig.* **68** 177
[20] Phan M H and Yu S C 2007 *J. Magn. Magn. Mater.* **308** 325
[21] De Oliveira N and Von Ranke P J 2010 *Phys. Rep.* **489** 89
[22] Tishin A 2007 *J. Magn. Magn. Mater.* **316** 351
[23] Gottschall T, Skokov K P, Fries M, Taubel A, Radulov I, Scheibel F, Benke D, Riegg S and Gutfleisch O 2019 *Adv. Energy Mater.* **9** 1901322
[24] Tang X, Sepehri-Amin H, Terada N, Martin-Cid A, Kurniawan I, Kobayashi S, Kotani Y, Takeya H, Lai J and Matsushita Y 2022 *Nat. Commun.* **13** 1817
[25] Tegus O, Brück E, Buschow K and De Boer F 2002 *Nature* **415** 150
[26] Yin Z, Wang J L, Wang J, Li J, Zhou H, Zhang C, Zhang H, Zhang J, Shen F and Hao J 2022 *ACS Nano* **16** 14632
[27] Zhang J, Chen X, Wang M, Zhang Q, Shi W, Zhan X, Zhao M, Li Z, Zheng J and Zhang H 2023 *Adv. Funct. Mater.* **33** 2306434
[28] Wang Y, Zhang X, Liu Y Q, Zhang J X and Yue M 2020 *Chin. Phys. B* **29** 067201
[29] Edalatpour S, Desutter J and Francoeur M 2016 *J. Quant. Spectrosc. Radiat. Transfer* **178** 14
[30] Sun F H, Ma S, Zhao W, Li C, Sang X, Wei P and Zhang Q 2021 *Rep. Prog. Phys.* **84** 096501
[31] Yan W, Nie X, Ke S, Hu Y, Ai X, Zhu W, Zhao W and Zhang Q 2022 *Adv. Funct. Mater.* **32** 2209739
[32] Xie H, Zhao L D and Kanatzidis M G 2024 *Interdiscip. Mater.* **3** 5
[33] Uchida K I, Zhou W and Sakuraba Y 2021 *Appl. Phys. Lett.* **118** 140504
[34] Edmund C S 1950 *Rep. Prog. Phys.* **13** 83
[35] Ma Z, Wei J, Song P, Zhang M, Yang L, Ma J, Liu W, Yang F and Wang X 2021 *Mater. Sci. Semicond. Process.* **121** 105303
[36] Tang X, Li Z, Liu W, Zhang Q and Uher C 2022 *Interdiscip. Mater.* **1** 88
[37] Gong Y, Sun J, Hu W, Li S, Xu W, Tan G and Tang X 2022 *Appl. Phys. Lett.* **120** 023905
[38] Gao Z, Chen J, Zhang Z, Liu Z, Zhang Y, Xu L, Wu J and Luo F 2023 *Adv. Electron. Mater.* **9** 2200823
[39] Kanchana V, Vaitheeswaran G and Rajagopalan M 2002 *J. Magn. Magn. Mater.* **250** 353
[40] Purwar S, Low A, Bose A, Narayan A and Thirupathaiah S 2023 *Phys. Rev. Mater.* **7** 094204
[41] Hamad M K, Maswadeh Y, Martinez-Teran E, El-Gendy A and Ziq K A 2021 *Eur. Phys. J. Plus* **136** 516
[42] Dijkstra J, Weitering H, Van Bruggen C, Haas C and De Groot R 1989 *J. Phys.: Condens. Matter* **1** 9141
[43] Hong M, Chen Z G, Yang L and Zou J 2016 *Nano Energy* **20** 144
[44] Wei T R, Qiu P, Zhao K, Shi X and Chen L 2023 *Adv. Mater.* **35** 2110236
[45] Perdew J P, Burke K and Ernzerhof M 1996 *Phys. Rev. Lett.* **77** 3865
[46] Kresse G and Furthmüller J 1996 *Phys. Rev. B* **54** 11169
[47] Bez H N, Yibole H, Pathak A, Mudryk Y and Pecharsky V K 2018 *J. Magn. Magn. Mater.* **458** 301
[48] Luo Z Z, Hao S, Cai S, Bailey T P, Tan G, Luo Y, Spanopoulos I, Uher C, Wolverton C and Dravid V P 2019 *J. Am. Chem. Soc* **141** 6403
[49] Kobayashi M 1990 *Solid State Ion.* **39** 121
[50] Xie W, He J, Zhu S, Su X, Wang S, Holgate T, Graff J, Ponnambalam V, Poon S and Tang X 2010 *Acta Mater.* **58** 4705
[51] Bergman D J and Levy O 1991 *J. Appl. Phys.* **70** 6821